Bi-component conformal electrode for radiofrequency sequential ablation and circumferential separation of large tumours in solid organs

Wang, Zhigang; Luo, Hongyan; Coleman, Stuart; Cuschieri, Alfred

Published in:
IEEE Transactions on Biomedical Engineering

DOI:
10.1109/TBME.2016.2573043

Publication date:
2016

Document Version
Peer reviewed version

Bi-component conformal electrode for radiofrequency sequential ablation and circumferential separation of large tumours in solid organs

Wang, Zhigang; Luo, Hongyan; Coleman, Stuart; Cuschieri, Alfred

Published in:
IEEE Transactions on Biomedical Engineering

DOI:
10.1109/TBME.2016.2573043

Publication date:
2016

Document Version
Peer reviewed version

Bi-component conformal electrode for radiofrequency sequential ablation and circumferential separation of large tumours in solid organs: development and in-vitro evaluation

Zhigang Wang*, *Senior Member, IEEE*, Hongyan Luo, Stuart Coleman, and Alfred Cuschieri*

***Abstract*— Objective*:* Complete destruction of large tumours by radiofrequency ablation (RFA) with surrounding tumour-free margin is difficult because of incomplete or non-uniform heating due to both heat sink effect of circulating blood and limitations of existing RF electrode design. A new RF electrode is described to overcome this limitation. *Methods:* A bi-component conformal (BCC) RFA probe providing sectorial sequential ablation followed by circumferential cutting is designed and evaluated. Three-dimensional finite-element analysis model was developed with temperature feedback-controlled simulation of RFA for electrode design and optimization. The prototype bipolar BCC probe with 3 embedded thermocouples was constructed and evaluated in tissue-mimicking phantoms. *Results:* Maximum tissue temperature was kept < 100 °C with power applied < 15 W. A 10 min ablation time was used for each sequence and after four sequential RFA, a large ablation zone of 55 cm^3 was achieved. Our experiment confirmed that lesions exceeding 3.7cm could be ablated and separated from the surrounded tissue. *Conclusion:* The new BCC probe is thus capable of controlled ablation followed by circumferential separation of the lesions, when required. *Significance:* The results of these experiments provide proof of concept validation that the BCC probe has the potential to ablate by sequential heating tumours in solid organs > 3.5cm then separate them by electrosurgical cutting from the surrounding normal parenchyma. The combined RF ablation and physical separation could completely destroy the cancer cells at the ablation site thus avoid any local recurrence of cancer. It requires further in-vivo validation studies in large animals.**

***Index Terms*—Bipolar electrode, finite element method (FEM), radiofrequency ablation (RFA), tissue-mimicking phantom.**

Manuscript received March 14, 2016; revised April 21, 2016; accepted May 21, 2016. This work presents independent research funded by the National Institute for Health Research (NIHR) under the Invention for Innovation (i4i) Programme (Project No: II-FS-0110-14001). The views expressed in this article are those of the authors and not necessarily those of the NHS, the NIHR or the Department of Health. Asterisk indicates corresponding author.

*Z. Wang, S. Coleman and *A. Cuschieri are with the Institute for Medical Science and Technology (IMSaT), University of Dundee, Wilson House, 1 Wurzburg Loan, Dundee Medipark, Dundee, DD2 1FD, UK (correspondence e-mails: z.z.wang@dundee.ac.uk; a.cuschieri@dundee.ac.uk). H. Luo is now with Bioengineering College, Chongqing University, Chongqing 400030, China.

I. Introduction

TUMOUR ablation is defined as the destruction of focal tumours by direct application of chemical agents or thermal energy [1]. Although surgical resection is still considered the gold standard treatment for primary disease, image-guided thermal ablative therapies, including radiofrequency ablation (RFA), interstitial microwave and laser, and high-intensity focused ultrasound, are in established use as adjuncts or as alternatives to surgical excision. RFA is the most common in-situ ablative technology in current clinical practice [2], which is mostly performed for primary hepatocellular cancer (usually in cirrhotic patients) and secondary liver tumours, from metastatic colorectal [3,4], renal cell [5] and bronchial cancers[6].

In RFA, an electrode is placed in the tumour to deliver radiofrequency current (normally in the 375 to 500 kHz range) in order to generate heat, thereby inducing thermal coagulative necrosis. The existing RFA electrodes and systems come in various designs and configurations. The 17-gauge needle electrode (Cool-tip RFA, Valleylab-Covidien, USA) is a FDA approved monoploar RFA system for ablation of non resectable liver tumours with an active tip of 2 - 3 cm [7]. It can be configured as a cluster of three needles. Other monopolar RFA systems use a mother probe which carries and deploys an array of electrodes exemplified by the RITA needle (RITA Medical System, Inc., USA) [8] or umbrella-shaped array such as the LeVeen electrode [9, 10] from Boston Scientific (www.bostonscientific.com). Tissue impedance and/or in-situ temperature measurement are used to provide feedback to control RF energy output. Bipolar RFA systems are based on twin electrodes at the tip of RFA needle, e.g., Celon Pro Surge applicator (Celon AG Medical Instruments, Teltow, Germany) [11]. Multipolar RFA electrode systems have also been proposed consisting of multiple single needle electrodes [12]. RFA can be applied percutaneously with image guidance by CT, MRI or external ultrasound; or

laparoscopically with visual guidance and laparoscopic contact ultrasound scanning.

All these existing RFA technologies suffer various limitations, which may result in incomplete destruction of tumours. These relate to accuracy of image guidance (e.g., accuracy of probe placement by current ultrasound guidance), and effective technology for in situ ablation which overcomes the heat sink effect of flowing blood in neighbouring blood vessels, and charring of the RFA probe[13]. Charring becomes a major problem during ablation of large tumour as the carbonisation prevents current flow from the probe to the tumour tissue. Local recurrence of cancer at the ablation site is reported in 20% of cases, particularly for lesions exceeding 3.0 cm [14]. The present study aimed to develop a new RFA device which reduces electrode charring by more uniform heating and applies sequential heating in order to achieve large and complete ablation with adequate tumour free margins. The device utilizes an electrode which conforms to the size of the target lesion and avoids collateral damage to surrounding healthy tissue. When required, the ablated tumour can be also separated from the surrounding tissue by electrosurgical cutting thus provide complete destruction of the whole ablated cancer. This report describes our proof-of-concept RFA technology development and evaluation.

II. Methods and Materials

A. RFA Electrode Probe with Sequential Heating Concept

The BCC probe for RFA electrode was designed and constructed in house. Figure 1 illustrates the BCC probe design (Fig. 1a-c) and proposed RF heating concept for both ablation (Fig. 1d) and separation by electrosurgical cutting (Fig. 1e). The BCC probe has two component electrodes, one of which can be extended in a loop (Fig. 1b-c) from the centre to periphery of the lesion. This permits bipolar RFA for localised heating of the tissue between the two electrodes, i.e., current flows from the deployable loop electrode to the central, fixed electrode.

Multiple deployable electrodes could be arranged in various configurations, such as a symmetric configuration consisting of two deployable electrodes, however the current version outlined in Fig 1 is designed for large volumetric ablation using a single deployable loop electrode configuration. When in use, the BCC probe is first inserted into the centre of the tumour mass with the loop electrode retracted (Fig. 1a). In the 1st sequence (S1), the loop electrode is deployed (assisted by electrosurgical cutting) until it reaches the peripheral margin of the tumour. Bipolar RFA is then performed to ablate a quadrant of an ellipsoid tumour volume (Fig. 1d). The loop electrode is then retracted back to the closed position and rotated by 90°to next (i.e. 2nd) position. Again, the loop electrode is deployed to the periphery and RF ablation is performed (S2). Four sequences (S1 – S4) are illustrated for four quadrant ablation of an ellipsoid tumour (Fig. 1d). Finally, when considered necessary, an additional sequence (S5) for RF-assisted perimeter cutting circumferentially incises the margin around the tumour, separating it from the surrounding healthy parenchyma (Fig. 1e).

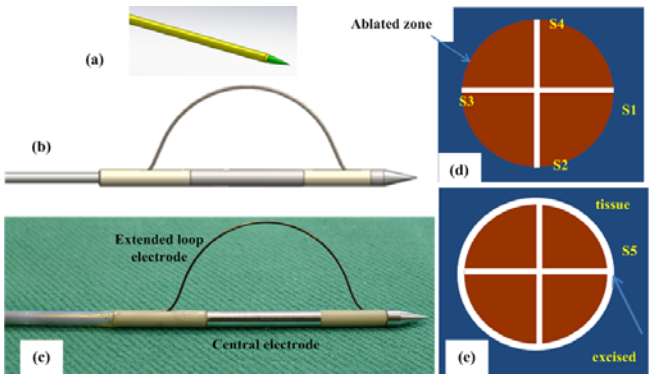

Fig. 1. RFA electrode probe and proposed RFA heating concept: (a-b) 3D CAD drawing showing probe design with the limb electrode retracted (a) and extruded and deployed (b); (c) a photograph of the constructed probe prototype, (d) illustration of a sectional view (from top at probe distal point) of the proposed RF ablated area with four sequences (S1-S4) with 90 degree probe rotation between each sequence, (e) with additional sequence (S5) for RF perimeter cutting to excise and separate the ablated zone from the surrounding healthy tissues.

B. 3D FEM Modelling

Although other numerical methods, such as finite difference model [15] or radial basis collocation method [16], have been used in RFA simulation, finite element method (FEM) has been the most widely used and accepted method. FEM modelling was used to analyses radiofrequency cancer ablation [17] by solving RF Joule (resistive) heating and Penne's bio-heat equation [18]. FEM modelling was further used to study the influence of blood vessel on the thermal lesion formation (the heat sink effects) during RFA [19] and the influence of other parameters such as water evaporation [20] and tissue conductivities with efficient RFA experiment design [21, 22]. In this study, an anatomical 3D FEM model was used for RFA simulation. In brief, an explanted Thiel-embalmed cadaveric liver (IRIS L-Liver-FEB-2011) was scanned using an MRI scanner (Fig.2a), and subsequently the 2D MRI sliced images were segmented (Fig.2b), smoothed and converted into a 3D (Fig.2c) Computer Aided Design (CAD) liver model (using ScanIP+FE_CAD, Simple ware Ltd, UK). A CAD package (Solidworks) was used to combine the 3D liver geometry with the BCC probe model at a pre-planned deployment position.

A FEM package (COMSOL Multiphysics, UK) was used to simulate and predict the tissue ablation zone within the organ (Fig. 2d). In particular, Penne's equation [18] below was used to simulate heat distribution in tissues.

$$\rho C \frac{\partial T}{\partial t} + \nabla \cdot (-k\nabla T) = \rho_b C_b \omega_b (T_b - T) + Q_{ext} + Q_{met} \quad (1)$$

where ρ indicates tissue density in (kgm^{-3}), C indicates specific heat capacity of tissue at constant pressure ($Jkg^{-1}K^{-1}$), k indicates thermal conductivity ($Wm^{-1}K^{-1}$), T is temperature

(K), ρ_b indicates density of blood (kgm^{-3}), C_b indicates specific heat of blood (Jkg^{-1}K^{-1}), ω_b indicates blood perfusion (=6.4e^{-3} 1/s) and T_b indicates temperature of blood (K). Term Q_{met} indicates contribution of heat due to tissue metabolic activities which in this case is significantly smaller than the RF heat source thus set to 0 in the model, and Q_{ext} indicates heat source due to external RF spatial heating source (Wm^{-3}). All the properties can be found from literature [23]. The ablation zone was estimated using an iso-thermal plot for a tissue temperature of 50°C and above [15, 21] since heating of tissue at 50°C and above will produce irreversible cellular damage and result in ablation [24, 25].

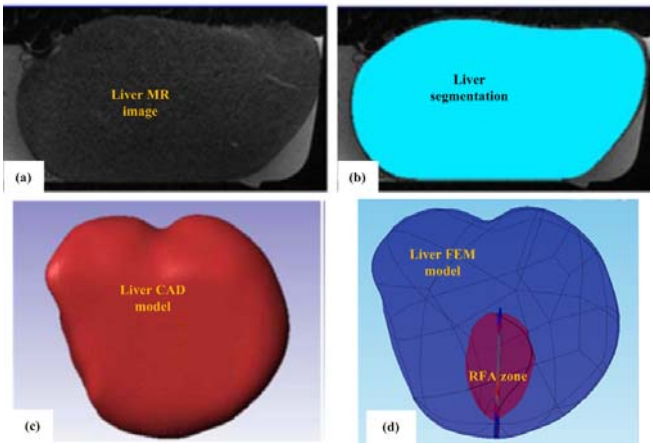

Fig. 2. Illustrations of an anatomic 3D FEM modelling: (a) One MRI slice of an explanted Thiel-embalmed cadaveric liver, (b) segmentation of the MRI sliced images, (c) converted into a 3D CAD liver model, and (d) Combination of the 3D liver model with an extruded RF electrode probe in FEM RFA simulation, probe design optimisation and validation.

FEM simulation was also used for the design of the RF electrode probe, its optimisation and validation. Thus, FEM simulation of thermal distribution was used to minimize hot spots for uniform ablation, determine the appropriate thermocouple integrated locations. Specifically for bipolar cutting, it was desirable to make the surface area of the loop electrode small compared to the central electrode; this combination ensures that the deployable electrode would heat rapidly and to a higher temperature than the central one. Furthermore, the outer electrode had to be scaled so that it was sufficiently flexible to be deployed but also large enough to be sufficiently strong and rigid to cut tissue.

C. Temperature-Controlled RFA in FEM Modelling

In the RFA FEM modelling, we aimed to keep maximal tissue temperature (T_{max}) below 100 °C to avoid tissue carbonization. Hence, the control target temperature T_{ct} was set at 90 °C, although other values below 100 °C may be used as long as T_{max} was kept below 100 °C. Algorithms (outlined below) were used to control RF output voltage V within a pre-prescribed ablation volume or treatment time t_{pt}:

$$v = v_0 + w_1(T_{ct} - T_{\max}) \quad \text{if } T_{max} <= T_{ct} \tag{2a}$$

or

$$v = v_0 + w_2(T_{ct} - T_{\max}) \quad \text{if } T_{max} > T_{ct} \tag{2b}$$

where v_0 is the initial applied RF voltage, w_1 is voltage increase scale factor and w_2 is voltage decrease scale factor. For this simulation, we used following values: v_0 =30 V, w_1 =0.2, w_2 =5, and T_{ct} = 90 °C.). If T_{max} was smaller than T_{ct} (= 90 °C), then the equation (2a) was used to calculate the value of the applied voltage which will increase slowly (scale factor w_1 =0.2) from its original value v_0 (=30 V). If T_{max} was larger than T_{ct} (= 90 °C), then the equation (2b) was used to calculate the value of the applied voltage which will decrease quickly (scale factor w_2 =5) from its original value v_0 (=30 V). This would ensure the ultimate maximal tissue temperature will never exceed 100 °C.

The generated RF power density (Wm^{-3}) can be obtained from Q_{ext} = J·E where J is the current density (Am^{-2}) and E is the electric field (Vm^{-1}). The values of these two vectors are derived from solving Laplace's equation below

$$\nabla \cdot (\sigma \nabla V) = 0 \tag{3}$$

where σ stands for electrical conductivity of tissue (Sm^{-1}) and V is the applied voltage (V). In our modelling, we used temperature-dependent σ [26] with initial σ = 0.148 (Sm^{-1}) for liver tissue at 500 kHz and body temperature 37 °C [27].

D. RFA Evaluation Using Infrared Thermal Camera for Temperature Monitoring

Infrared (IR) thermographic imaging was previously reported by our group [28] to monitor the thermal spread causing collateral damage during energised dissections in laparoscopic and open operations. Hsiao et al [29] used IR imaging to determine the tissue temperature, lesion formation and overheating during high-intensity focused ultrasound (HIFU) thermal tissue ablation. Although IR imaging is more reliable for surface temperature mapping due to its penetration limit, we believe that it can provide important thermal information during RFA ablation, especially when combined with monitoring by in-situ thermocouples.

Throughout the development of the BCC probe and its evaluation, an IR thermal camera (JADE, Cedip Infrared Systems Ltd, France) was used to monitor the heating by the probes and its distribution, estimate the ablation zone and identify hot spots or thermal leaks.

E. Electrode Prototype with Integrated Thermocouples

The final bipolar prototype (Fig. 3) with three integrated thermocouples has an outside diameter of 3mm and designed to ablate and resect a lesion with a range of sizes, up to a maximum lesion diameter of around 3.7 cm.

The device has two electrodes (Fig. 3a-b); the central electrode is made from stainless steel and has dimensions of Ø3x22mm. It is connected to a high-temperature resistant wire which runs inside the instrument to its proximal end, and to insulating polymer components. The deployable loop

electrode is made of nickel-titanium alloy wire with Ø 0.5mm. The wire is formed into an approximately semi-circular shape by heat-treatment. When retracted this wire will lie alongside the central electrode, but when deployed, it will return to its set shape due to the super-elastic effect. This effect allows the wire to undergo large strains during deployment without sustaining metal fatigue, thus a relatively large and stiff electrode can be deformed into a range of shapes. The heat treatment of the loop electrode has been selected to ensure that it remains super-elastic when heated during ablation.

A 30% glass-fibre filled PEEK (Fig. 3a) was used to produce insulating components due to its high strength and rigidity and good high-temperature performance. The devices shaft and point are made of stainless steel. Thermocouples are integrated into the prototype at key locations (Fig. 3b,c) to allow temperature monitoring during use. The instrument shaft is approximately 200mm long (Fig. 3d). The handle allows for controlled deployment of the loop electrode and allows electrical connections to be plugged in.

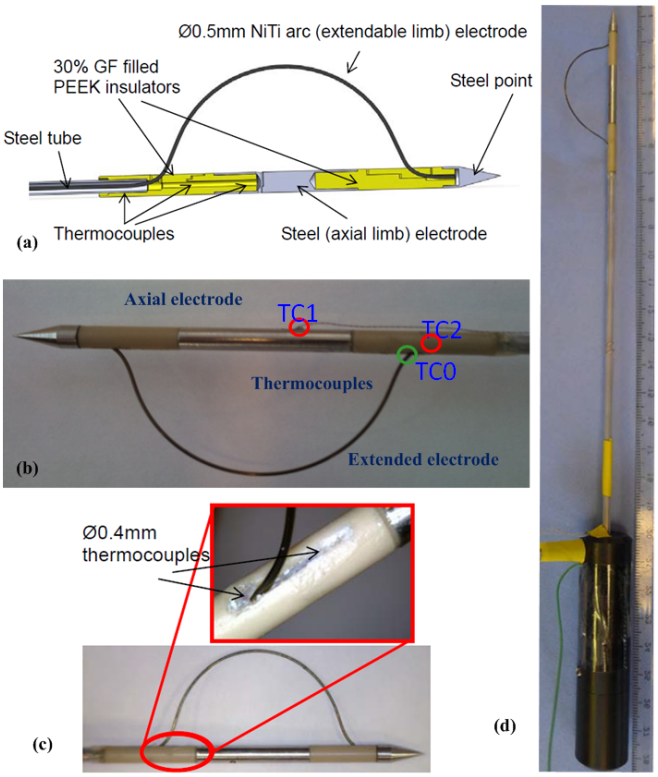

Fig. 3. Final electrode prototype for RFA evaluation using phantoms: (a) Sectional view of distal end of the prototype in CAD drawing with the deployable NiTi electrode in its extended position, and photographs showing the constructed prototype with thermocouples highlighted (b,c) and the whole prototype with the external handle (d).

F. Experimental Evaluation

In experimental evaluation, three small thermocouple sensors (TC_0, TC_1, TC_2) were attached to the probe shaft at locations determined previously by the FEM simulation study: TC_0 on inside edge of the extruded limb electrode for recording temperature to ensure ablation up to perimeter; TC_1 located on central electrode, recording maximal temperature for control of RF generator, keeping temperature below 100 °C; and TC_2 located at outer edge of the extruded limb electrode, monitoring temperature spread to the surrounding healthy tissue.

Due to its high electrical conductivity, a Thiel-embalmed liver was not suitable for experimental evaluation of RFA [30]. Additionally, a condition of the funding was that animal tissue should not be used for experimentation. Therefore, tissue-mimicking gel was produced to provide a tissue phantom for experimentation [31]. The materials used to fabricate this gel included polyacrylamide mixed with bovine serum albumin (BSA), a protein used as a temperature-sensitive indicator [32].

A commercial electrosurgical RF generator (DRE ASG-300, DREMED, 1800 Williamson Court, Louisville, USA) was used for all experimental evaluation. The generator has the capability of delivering 120 W up to 1000 Ω when used in pinpoint coagulation monopolar operation and 40 W up to 500 Ω for bipolar mode at a frequency of 490 kHz ± 5 kHz. However, there is no temperature feedback control in this generator, and all the controls were done manually by hand switch off/on the generator depended on separate PC's temperature recording monitored visually by the authors.

III. Results

A. FEM Simulation Demonstrated Sequential RFA Resulting in Large Ablation Zone

Figure 4 shows RFA simulation results from a bipolar electrode probe. Figure 4(a-d) are various plots for one ablation sequence. Figure 4(a) demonstrates our temperature-controlled FEM simulation (maximal temperature kept below 100 ^{0}C) with variable applied voltage for 10 min (one RFA sequence). Figure 4(b) plots the corresponding applied RF power (from 15.5 to 5.5 W with a mean of 6.9 W) and the temperature-dependent liver resistance (from about 101 to 77 Ω with a mean of 81 Ω). A slice plot in Fig. 4(c) shows the temperature distribution and a 3D iso-thermal surface plot in Fig. 4(d) illustrates a RFA zone with temperature ≥ 50 ºC. Figure 4(e1-4) illustrate 4 RFA activated sequences with three 90 degree rotations of the probe shaft. After 4 sequences, an ellipsoid RF ablation zone (temperature ≥ 50 ºC) of 4.7cm diameter (volume of 54.8 cm^3) is produced (Fig. 4f). The treatment margin is well defined as the locus described by the extended loop limb electrode. This was a simplified FEM model since in-vivo the liver is a very complex electrical and thermal organ due to its inhomogeneity and three different types of blood vessels of different diameters and flow velocities. FEM models used to study the influence of blood vessel can be found from literature such as [19]. We also realize that FEM modelling has its accuracy limitation in mesh size selection. The mesh used in our model was finer at electrodes (minimum of 0.01 mm) and was normal for other

locations with total number of elements around 80,000. A further mesh refinement study would provide more accurate results.

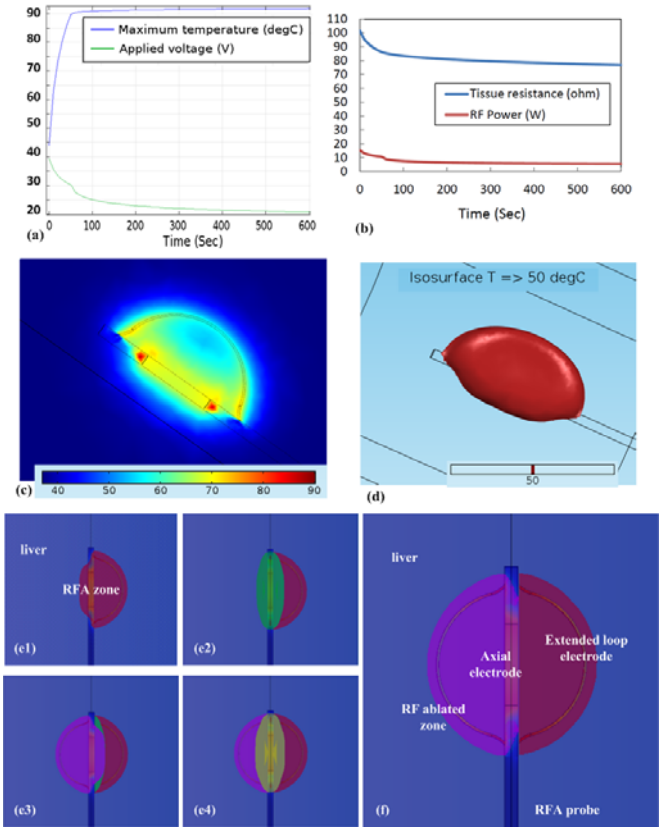

Fig. 4. RFA FEM simulation using an anatomic 3D liver model (details in Fig. 2): (a) Temperature-controlled applied voltage in one sequence, (b) Temperature-dependent liver electrical resistance and applied power, (c) temperature slice plot and (d) iso-thermal surface plot in one sequence; (e1-4f) Four sequential RFA with 90 degree probe (axial) shaft rotation each to achieve a ellipsoid ablation zone (f) for final BCC bipolar electrode. The extended limb electrode can be extruded conformably to the tumour periphery (under image guidance).

B. RFA Evaluation using Tissue Mimicking Gel Phantom

Figure 5 are IR thermographic imaging study used for electrode probe development and RFA evaluation using a gel phantom at room temperature. The probes were inserted into the gel phantom at depth of 5mm from the top imaging surface. Fig. 5(a) shows faulty thermal insulation at the probe shaft in one early prototype (10 W, 30 sec) which could cause injury to surrounding healthy tissue. Altered prototype construction eliminated this problem, and Fig. 5(b) demonstrates that thermal distribution at 10 W & 10 min was confined into the intended area between the two electrodes. However, there was a slightly hot spot outside the target ablation area (Fig. 5b), and this was monitored by two thermocouples (Fig. 3, TC0, TC2) for safety. Fig. 5(c) demonstrates a monopolar application (10 W and 1 min) to the extended loop electrode to generate higher temperature (around or >100 ºC) in order to facilitate circumferential excision/separation of the ablated tissue from surrounding healthy tissue. We realized that temperature measured by IR imaging in our setup (i.e., electrodes inserted and located 5 mm depth from the measuring surface of the gel phantom) was lower than that from in-situ temperature, we found that there was about 15 ºC difference by comparing an in-situ thermocouple measurement.

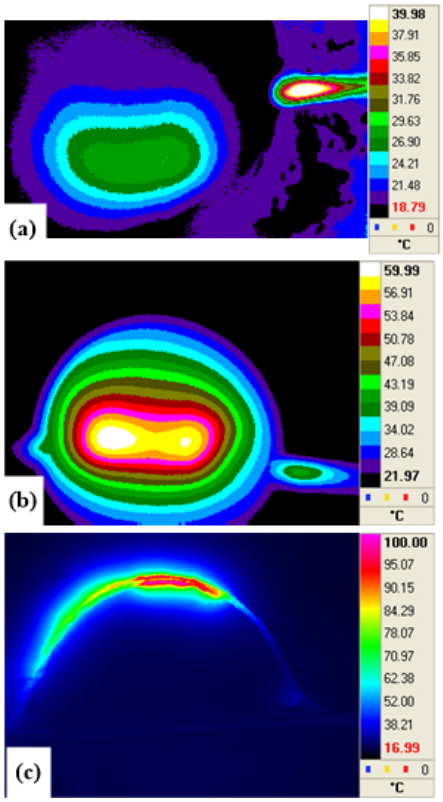

Fig. 5. RFA thermal distribution study using tissue mimicking gel phantom and IR thermal camera with applied 10 W: (a) RFA at 30 sec demonstrated a fault in shaft thermal insulation in one early electrode prototype, (b) RFA at 10 min demonstrated RFA zone at intended area, (c) RFA with higher temperature at 1 min using monopolar application (electrosurgical cutting) for facilitating separation of the ablated tissue from surrounding tissue.

The final prototype probe was inserted into a gel phantom for sequential RFA evaluation (Fig. 6). The ablated gel turns from transparent to ivory white at a coagulation temperature > 50 ºC (Fig. 6a-c). This is in agreement with the in-situ temperature monitoring during RFA (Fig. 6d). A planned RFA sequence was completed when the margin was heated > 50 ºC as monitored by thermocouple TC_0 while maintaining T_{max} < 100 ºC from monitored by thermocouple TC_1, whist temperature of surrounding healthy tissue monitored by TC_2 remained < 45 ºC. Following rotation of probe sequential RFA in four sequences, each lasting 10 min, and an ellipsoid RF ablation zone was created. This could be separated by circumferential cutting from the surrounding normal zone (Fig. 6c). The ablated and separated volume measured 4.3 cm axially and 3.7 radially, corresponding to the deployed loop electrode dimensions.

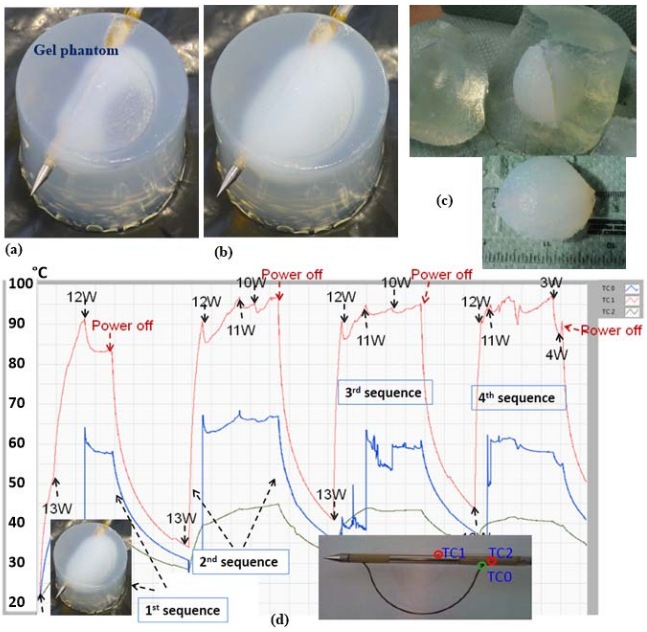

Fig. 6. RFA evaluation using tissue mimicking gel phantom: photographs showing (a) an early state of 1st sequence RFA with some coagulated gel turning into ivory white, (b) near the end of 1st sequence with coagulated gel spread the whole intended area, (c) at the end of RFA evaluation after 4 rotational sequences and additional cutting sequence, an ablated and separated volume measured > 3.7cm diameter, (d) real-time temperature recording of the 4 RFA sequences with RF power output changes.

C. Evaluation of RF-assisted Perimeter Excision Using Potato Phantom

Although our gel phantom evaluation results have demonstrated both RF ablation and excision by the BCC probe (Fig. 6), we realize that this gel phantom though accurate in RF heating, is not a suitable medium for studying the excision of the ablated tissue. For this, a much harder natural material (potato) model was used in the present study. To excise the hard potato tissue, the Cut mode of the electrosurgical generator was used for the Bi-component electrode, i.e., the extended electrode functions as the cut electrode while the axial electrode as the 'conventional' return electrode. This was achieved due to the generator's Cut I mode which generates constant output power over a wide range of impedances (e.g., it can deliver 150 W up to 2250 Ω). Several experiments on potatoes demonstrated that electrosurgical cutting could be adapted and used with the BCC probe. Photographs in Fig. 7 showed the excised potato volume achieved with the BCC probe using 100 W in Cut I mode (the generator can deliver 100 W constant for a wider load up to 3000 Ω).

The amount and site of carbonisation observed with the BCC probe during RF potato cutting was quite variable and depended on factors including RF power settings, cut speed, and temperature of the material. The best results were achieved when cutting was carried out rapidly and with relatively high power. This is under further investigation in on-going experiments on RF power and waveform, and RF multipolar configuration.

There are some potential challenges with deploying the conformal electrode portion into harder tissues such as unable to extend the conformal electrode and/or deployed in a deformed loop shape which would result in inaccurate ablation zone. The Cut mode mentioned above could be used to facilitate the deployment although a smaller power would be preferred in order to reduce electrode carbonization. The super-elastic material used in the loop electrode of our final prototype (described in section E of II) provided us the required electrode loop shape with relatively large stiffness, in particular under electrosurgical current heating due to its heat treatment in shape memory alloy. In the future, other sharp geometrical structure such as including a razor blade at the loop electrode could be designed to mechanically cut through the tissue for deployment and excision. Also, in order to avoid any carbonization, other electrosurgical power mode could be investigated, e.g., the blend mode which is a combination of cutting and hemostasis and with a range of settings for different cutting effect.

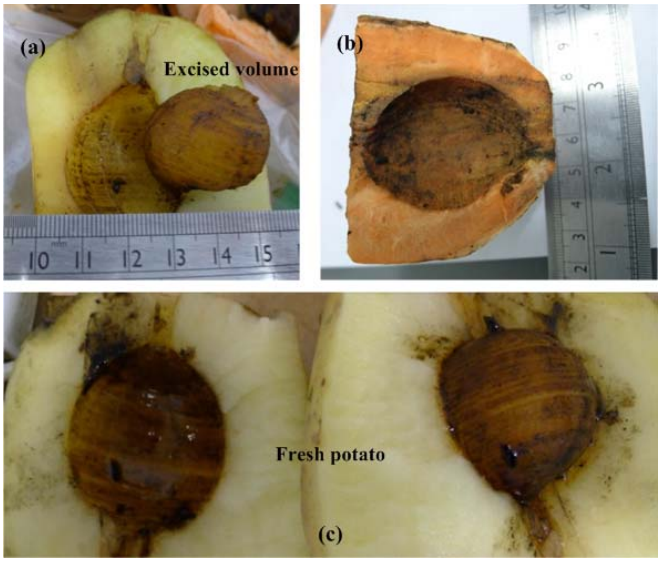

Fig. 7. Photographs showing fresh potato models used for RF-assisted cutting evaluation of our electrode probe: all testing was successful with RF cut and separated ellipsoid potato volume the same as the planned and deployed electrode perimeter cutting geometry.

IV. Conclusion

Complete destruction of large tumours by radiofrequency ablation (RFA) is difficult because of incomplete or non-uniform heating due to both heat sink effect of circulating blood and limitations of existing RF electrode design. The results of these experiments provide proof of concept validation that the BCC probe has the potential to ablate by sequential heating tumours in solid organs > 3.5cm and then separate them by electrosurgical cutting from the surrounding normal parenchyma. The physical separation could further

destroy any remaining viable cancer cells at the ablation site thus avoid any local recurrence of cancer. However, there are limitations in the present study by our simplified tissue models both in FEM modeling and ex-vivo evaluation. An ex-vivo animal organ model with simulated blood perfusion using an already in-house heart-lung machine (Jostra HL30, MAQUET, Germany) is our immediate follow-on study. However, it requires further in-vivo validation studies in large animals and will require future work using an automated control system. The system could include a dedicated microprocessor-based circuitry for output of any RF waveforms and sequences and an RF power amplifier for RF electrode in tissue ablation and cutting, real-time electrode-tissue impedance and monitoring real-time ablation temperature from in-situ thermocouples.

ACKNOWLEDGMENT

The authors would like to acknowledge the assistance of MR imaging of the explanted Thiel-embalmed cadaveric liver by Dr M Gueorguieva at IMSaT, University of Dundee.

REFERENCES

[1] S. N. Goldberg et al., "Image-guided Tumor Ablation: Standardization of Terminology and Reporting Criteria," Radiology, vol. 235, pp. 728-739, 2005.

[2] Standards for radiofrequency ablation (RFA), 2nd ed.. The Royal College of Radiologiest, London, 2013, pp 1-8.

[3] A. E. Siperstein et al., "Survival after radiofrequency ablation of colorectal liver metastases: 10-year experience," Ann Surg, vol. 246, pp. 559-65; discussion 565-7, Oct 2007.

[4] Y. Minami and M. Kudo, "Radiofrequency Ablation of Hepatocellular Carcinoma: A Literature Review," International Journal of Hepatology, vol. 2011, 2011.

[5] T. M. Wah et al, "Radiofrequency ablation (RFA) of renal cell carcinoma (RCC): experience in 200 tumours," BJU Int, vol. 113, pp. 416-28, Mar 2014.

[6] J. Ferguson et al, "Long term results of RFA to lung metastases from colorectal cancer in 157 patients," Eur J Surg Oncol, Feb 4 2015.

[7] D. Wang et al, "Four-dimensional Transcatheter Intra-arterial Perfusion MRI Monitoring of Radiofrequency Ablation of Rabbit VX2 Liver Tumors," Journal of magnetic resonance imaging : JMRI, vol. 34, pp. 563-569, 2011.

[8] P. Abitabile and C. A. Maurer, "Radiofrequency ablation of liver tumors: a novel needle perfusion technique enhances efficiency," J Surg Res, vol. 159, pp. 532-7, Mar 2010.

[9] M. Koda et al, "Comparison between different thickness umbrella-shaped expandable radiofrequency electrodes (SuperSlim and CoAccess): Experimental and clinical study," Experimental and Therapeutic Medicine, vol. 2, pp. 1215-1220, Nov-Dec 2011.

[10] M. Hirakawa et al, "Randomized controlled trial of a new procedure of radiofrequency ablation using an expandable needle for hepatocellular carcinoma," Hepatology Research, vol. 43, pp. 846-852, 2013.

[11] U. Zurbuchen et al, "Ex Vivo Evaluation of a Bipolar Application Concept for Radiofrequency Ablation," Anticancer Research, vol. 29, pp. 1309-1314, 2009.

[12] S. Clasen et al, "Multipolar radiofrequency ablation using internally cooled electrodes in ex vivo bovine liver: correlation between volume of coagulation and amount of applied energy," Eur J Radiol, vol. 81, pp. 111-3, Jan 2012.

[13] B. M. Künzli et al, "Radiofrequency ablation of liver tumors: Actual limitations and potential solutions in the future," World Journal of Hepatology, vol. 3, pp. 8-14, 2011.

[14] A. Stang et al, "Selection criteria for radiofrequency ablation for colorectal liver metastases in the era of effective systemic therapy: a clinical score based proposal," BMC Cancer, vol. 14, p. 500, 2014.

[15] G. Zorbas, and T. Samaras, "A study of the sink effect by blood vessels in radiofrequency ablation," Computers in Biology and Medicine, vol. 57, pp. 182-186, 2015.

[16] M. Jamil, and E. Y. K. Ng, "Evaluation of meshless radial basis collocation method (RBCM) for heterogeneous conduction and simulation of temperature inside the biological tissues," International Journal of Thermal Sciences, vol. 68, pp. 42-52, 2013.

[17] D. Haemmerich et al., "Finite-element analysis of hepatic multiple probe radio-frequency ablation," IEEE Trans Biomed Eng, vol. 49, no. 8, pp. 836-42, Aug, 2002.

[18] H. H. Pennes, "Analysis of Tissue and Arterial Blood Temperatures in the Resting Human Forearm," Journal of Applied Physiology, vol. 1, no. 2, pp. 93-122, August 1, 1948, 1948.

[19] S. Payne et al, "Image-based multi-scale modelling and validation of radio-frequency ablation in liver tumours," Philosophical Transactions of the Royal Society of London A: Mathematical, Physical and Engineering Sciences, vol. 369, pp. 4233-4254, 2011.

[20] Q. Zhu et al., "Numerical study of the influence of water evaporation on radiofrequency ablation," Biomed Eng Online, vol. 12, pp. 127, 2013.

[21] E. Y. K. Ng, and M. Jamil, "Parametric sensitivity analysis of radiofrequency ablation with efficient experimental design," International Journal of Thermal Sciences, vol. 80, pp. 41-47, 2014.

[22] M. Jamil, and E. Y. K. Ng, "Quantification of the effect of electrical and thermal parameters on radiofrequency ablation for concentric tumour model of different sizes," Journal of Thermal Biology, vol. 51, pp. 23-32, 2015.

[23] S. Tungjitkusolmun et al, "Three-dimensional finite-element analyses for radio-frequency hepatic tumor ablation," Biomedical Engineering, IEEE Transactions on, vol. 49, pp. 3-9, 2002.

[24] I. D. McRury, and D. E. Haines, "Ablation for the treatment of arrhythmias," Proceedings of the IEEE, vol. 84, no. 3, pp. 404-416, 1996.

[25] S. N. Goldberg et al, "Thermal ablation therapy for focal malignancy: a unified approach to underlying principles, techniques, and diagnostic imaging guidance," AJR Am J Roentgenol, vol. 174, no. 2, pp. 323-31, Feb, 2000.

[26] I. A. Chang, "Considerations for thermal injury analysis for RF ablation devices," Open Biomed Eng J, vol. 4, pp. 3-12, 2010.

[27] C. Gabriel et al, "The dielectric properties of biological tissues: I. Literature survey," Physics in Medicine and Biology, vol. 41, no. 11, pp. 2231, 1996.

[28] C. Song et al, "Thermal spread and heat absorbance differences between open and laparoscopic surgeries during energized dissections by electrosurgical instruments," Surg Endosc, vol. 23, pp. 2480-7, Nov 2009.

[29] Y.-S. Hsiao et al, "Characterization of Lesion Formation and Bubble Activities during High Intensity Focused Ultrasound Ablation using Temperature-Derived Parameters," Infrared physics & technology, vol. 60, pp. 108-117, 2013.

[30] Z. Wang et al, "Electrical conductivity measurement in thiel-embalmed tissue model: relevance to radiofrequency ablation," Electronics Letters, vol. 50, pp. 1125-1127, 2014.

[31] Z. Wang et al, "Image-based 3D modeling and validation of radiofrequency interstitial tumor ablation using a tissue-mimicking breast phantom," International Journal of Computer Assisted Radiology and Surgery, pp. 1-8, 2012.

[32] B.-L. Zhang et al, "A polyacrylamide gel phantom for radiofrequency ablation," International Journal of Hyperthermia, vol. 24, pp. 568-576, 2008.